

Estimation of variance distribution in three-dimensional reconstruction. II. Applications

Weiping Liu*

*Wadsworth Center, New York State Department of Health, Albany, New York 12201-0509, and
Department of Physics, University of New York at Albany, Albany, New York 12222*

Nicolas Boisset

*Laboratoire de Biochimie Fondamentale, Université François Rabelais, and Unité de Recherche Associée au
Centre National de la Recherche Scientifique 1334, 2 bis Boulevard Tonnelle, 37042 Tours Cedex, France*

Joachim Frank

*Wadsworth Center, New York State Department of Health, Albany New York 12201-0509, and
Department of Biomedical Sciences, University of New York at Albany, Albany, New York 12222*

Received March 9, 1995; accepted July 5, 1995

A previously developed theory of three-dimensional (3-D) variance estimation [J. Opt. Soc. Am. A **12**, 2615–2627 (1995)] is applied to the structural study of a hemocyanin-Fab complex with the electron microscope. The precise locations of structurally variable regions of the macromolecule are determined from the 3-D variance maps. The structural differences among different classes of the macromolecular complex are assessed by the use of the statistical *t*-test, and the 3-D antibody binding sites are revealed. From a model analysis, a rule is demonstrated for visually identifying a 3-D conformational change by the inspection of the 3-D variance map. Our analysis lays the foundation for numerous practical applications of variance estimation in the 3-D imaging of macromolecules. © 1995 Optical Society of America

1. INTRODUCTION

In our previous paper,¹ a theory of three-dimensional (3-D) variance estimation was developed for the structural studies of single macromolecules that are reconstructed from their projections obtained from electron microscopy. Three approaches of estimating the projection noise were outlined that make use of redundancies in the data collection. From the resulting noise estimates, the 3-D variance of the reconstruction can be computed, provided that the reconstruction algorithm used is linear. This method of estimation is applicable in the practically important case of the random-conical reconstruction method (see brief introduction in the companion paper¹), which takes advantage of preferred orientations of the molecules on the specimen grid.

Here, by applying relevant tools of statistical testing to the 3-D variance estimates, we attempt to assess the reliability of local features found in a reconstruction and the significance of structural differences of two experimentally related reconstructions. The structural assessment is made more difficult by the existence of correlation among reconstruction voxels. One way to account for such an effect is through the resampling of the reconstructions to achieve approximate independence among the voxels. Another way is to compute the 3-D variances and to apply statistical tests to variance estimates obtained with different low-pass cutoff frequencies.

Subsequently we show how the information contained in the 3-D variance may be utilized in the application to experimental data. The power of combining classification analysis and 3-D reconstruction with 3-D vari-

ance analysis is demonstrated by the example of antibody binding to a hemocyanin molecule. Besides being useful for significance assessments, the 3-D variance distribution also provides information on the molecule's conformational changes.

2. SIGNIFICANCE ASSESSMENT OF THREE-DIMENSIONAL RECONSTRUCTIONS

In this section, we show how the information contained in the 3-D variance can be exploited for the significance assessment of local features in the reconstructions. It must be emphasized that the variance yields information not contained in resolution measures. Various practical definitions of resolution are based on an assessment of reproducibility in Fourier space.^{2–4} The characteristic resolution distance describes the smallest size of trustworthy features within the entire 3-D image. However, it cannot address the resolvability of individual features. Furthermore, it tells nothing about the reproducibility of the intensity at a given voxel and hence is unable to answer questions about the significance of observed differences between two independent 3-D images.

We follow the nomenclature used in Ref. 1. Specifically, spatial or spatial frequency variables understood to be 3-D are capitalized and those in two dimensions are set in lowercase.

A. Significance of Local Features in a Reconstruction

The presence of strong noise components in the projections, which propagate to the 3-D image, raises questions

about the reproducibility of individual features in this image. In practice, $b(\mathbf{R})$ is computed at discrete voxels \mathbf{R}_k , and we assume that, by the use of an appropriate sampling rate, $b_k = b(\mathbf{R}_k)$ will represent $b(\mathbf{R})$ in the structural analysis with acceptable fidelity. The noise component of a 3-D image at any \mathbf{R} is roughly Gaussian distributed. This assumption is justified because this noise component is the sum of a large number of independent projection-noise components. The local feature assessment is generally a multivariate statistical problem, which is made difficult by two factors: the corresponding statistical test has to be designed according to what question one wishes to address regarding a local feature, and the full noise statistics of a 3-D image requires knowledge of the joint probability density function of all voxels (which is determined by the variance of each voxel and covariance between all pairs of voxels, in the case of Gaussian-noise distribution of each voxel). Instead we have only estimates of the average $b(\mathbf{R}_k)$ and variance $\tilde{\nu}(\mathbf{R}_k)$ of each voxel. Although the covariance between any two voxels could in principle be estimated, its computation is quite cumbersome. These problems make the statistical assessment very complicated or even impossible.

There are two kinds of statistical tests, nonparametric and parametric. For a 3-D image $b(\mathbf{R})$, one cannot employ nonparametric rank-analysis methods⁵ because the sample populations at every \mathbf{R} do not exist. With the existing parametric statistical test methods, which could be employed for local feature assessment, independence or equal variance between voxels is required. However, the noise components between the voxels are correlated because of the correlation of noise between the pixels in each projection and because of the reconstruction process (interpolation, backprojection, weighting, and resolution filtration). This calls for use of the computationally cumbersome covariance. We circumvent the use of the covariance in the significance assessment of local features by resampling the 3-D image to achieve approximate independence between voxels.

1. Approximate Number of Degrees of Freedom of Local Features in a Reconstruction

In our companion paper,¹ it was shown that, if the projection noise $n^{(i)}(k, l)$ is independent among the pixels and its level is the same for all projections, the 3-D covariance will have the same appearance as the point-spread function (PSF) associated with the reconstruction procedure (Fig. 1). This conclusion roughly holds when $n^{(i)}(k, l)$ has a much shorter correlation range than $1/(2U_f)$ so that the finite values of the 3-D covariance originate mainly from the resolution filtration. In that case, we can achieve approximate independence among voxels by resampling the 3-D reconstruction on a coarser grid, and an assessment of local features can then be given.

The resolution low-pass filter¹ $F_0(\mathbf{U})$ has a width of $2U_f$ in the U_X-U_Y plane and an approximate width of $2U_f/\epsilon$ in U_Z direction (where ϵ is the elongation factor of the PSF¹). Therefore, if we resample the 3-D image with the sampling rates in the X and the Y directions,

$$T_{XY} = 1/(2U_f), \quad (2.1)$$

and the sampling rate in the Z direction,

$$T_Z = \epsilon T_{XY}, \quad (2.2)$$

Shannon's sampling rate requirement will be roughly satisfied. As shown in Fig. 1, such a resampling also makes the 3-D covariance roughly vanish between the resampled voxels, achieving approximate independence. This means that, for a feature within the volume V_0 in the 3-D image, the number of independent points or the number of degrees of freedom (NDF) of the local feature is approximately

$$m = V_0/(T_{XY}^2 T_Z). \quad (2.3)$$

Therefore, while approximately representing $b(\mathbf{R})$, the resampled 3-D image b_k possesses noise components that are independent among the voxels, a property that makes the subsequent statistical tests possible.

For statistical tests in Subsections 2.A.2, 2.A.3, and 2.B.1, we now turn to the discussion of the NDF of the 3-D variance estimate N_e , as defined by

$$\text{var}[\tilde{\nu}(\mathbf{R})] = \frac{1}{N_e} \nu^2(\mathbf{R}). \quad (2.4)$$

Recall that, in our companion paper,¹ we defined an efficiency coefficient for 3-D variance estimation as

$$\eta = \frac{\text{var}[\tilde{\nu}_0(\mathbf{R})]}{\text{var}[\tilde{\nu}(\mathbf{R})]}, \quad (2.5)$$

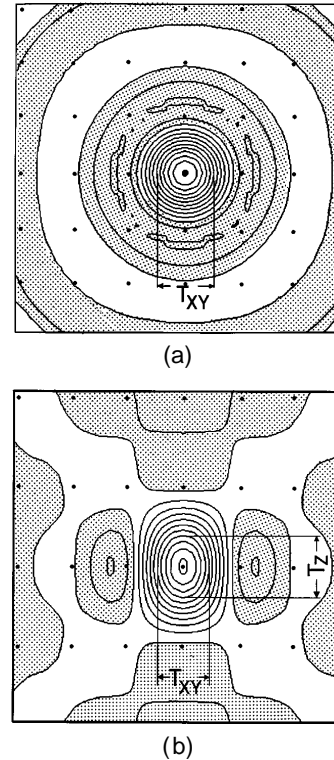


Fig. 1. Contour representation of the resolution filtration PSF function $h(R_{\perp})$, with missing cone angle $\theta_0 = 40^\circ$ and low-pass cutoff frequency of the filter $U_f = 1/(45 \text{ \AA})$: (a) central $X-Y$ plane, (b) central $X-Z$ plane. Shading indicates regions where $h(R_{\perp}) < 0$. The dots represent the resampling points with the sampling rates according to Eqs. (2.1) and (2.2). Note that $h(R_{\perp}) \approx 0$ in these points. [Contours in (a) are not completely circular because of numerical and sampling inaccuracies.]

where $\tilde{\nu}_0(\mathbf{R})$ is the sum of projection variance estimates $\tilde{\nu}_{wf}^{(i)}(\mathbf{r})$ that are considered independent of i . Hence, if we assume that the projection variance $\nu_{wf}^{(i)}(\mathbf{r})$ is equal for all projections, we obtain, by combining Eqs. (2.4) and (2.5),

$$\begin{aligned} N_e &= \eta \frac{\nu^2(\mathbf{R})}{\text{var}[\tilde{\nu}_0(\mathbf{R})]} \\ &= \eta \frac{N^2 \nu_{wf}^{(i)^2}(\mathbf{r})}{N \nu_{wf}^{(i)^2}(\mathbf{r})} \\ &= \eta N, \end{aligned} \tag{2.6}$$

where N is the number of projections. Because η is between 0.5 and 1,

$$N_e > N/2. \tag{2.7}$$

This result will be used in discussions below on statistical tests.

Next we turn to the assessment of local features. As mentioned above, depending on which aspect of a local feature in a 3-D image we wish to address, the necessary statistical test may be very different. Here we discuss two typical cases.

2. Significance of Variation within a Volume

If one wants to examine whether there are any significant structure variations within a chosen local volume V_0 , one has to test the null hypothesis H_0 : $b_1 = b_2 = \dots = b_m$, where b_k is the 3-D image value on the resampled voxels. The statistical F -test for multiple comparison⁶ can be used to assess the equality of the b_k 's in volume V_0 :

$$\hat{F} \equiv \frac{M_b}{M_w}, \tag{2.8}$$

where

$$\begin{aligned} \bar{b} &\equiv \frac{1}{m} \sum_{k=1}^m b_k \\ &\approx \frac{1}{n} \sum_{R_i \subset V_0} b(\mathbf{R}_i), \end{aligned} \tag{2.9}$$

$$\begin{aligned} M_b &\equiv \frac{1}{m-1} \sum_{k=1}^m (b_k - \bar{b})^2, \\ &\approx \frac{m}{m-1} \frac{1}{n} \sum_{R_i \subset V_0} [b(\mathbf{R}_i) - \bar{b}]^2, \end{aligned} \tag{2.10}$$

$$\begin{aligned} M_w &\equiv \frac{1}{m} \sum_{k=1}^m \tilde{\nu}_k \\ &\approx \frac{1}{n} \sum_{R_i \subset V_0} \tilde{\nu}(\mathbf{R}_i), \end{aligned} \tag{2.11}$$

n is the number of reconstruction voxels in volume V_0 , and $\tilde{\nu}_k$ is the 3-D variance estimate at the resampled voxel point b_k .

If $\hat{F} > F_{(v_b;v_w;\alpha)}$, reject H_0 at the α level, where $v_b = m - 1$ and $v_w = mN_e$ are the NDF of M_b and M_w , respectively.

Because, in practical 3-D reconstructions, the number of projections $N \geq 60$, $N_e > 30$ from relation (2.7). Thus $v_w \geq 60$ with $2 \leq m \leq 10$. Then, for the two commonly

used significance levels $\alpha = 0.05$ and $\alpha = 0.01$, the difference between the values of $F_{(v_b;v_w;\alpha)}$ for $v_w = \infty$ and $v_w = mN_e$ is less than 12%. Thus we can use $F_{(v_b;\infty;\alpha)}$ for $F_{(v_b;v_w;\alpha)}$ as the threshold to avoid having to estimate N_e . Also note that from relations (2.9)–(2.11), we can make the multiple comparison without actually resampling $b(\mathbf{R}_i)$ and $\tilde{\nu}(\mathbf{R}_i)$.

After one rejects H_0 and if one further wants to find which pairs of points are significantly different, one can employ the relevant test statistics for the assessment of linear contrasts and the multiple comparison of means.

3. Isolated Feature with Uniform Background

Suppose the reconstruction has an isolated feature in volume V_0 surrounded by a uniform background. The average value of the feature stands out from the background by a certain value. Then we wish to find out whether the feature is meaningful.

The difference between the average value of this feature and the background is

$$\begin{aligned} \Delta b_\nu &\equiv \bar{b}_\nu - b_0 \\ &= \frac{1}{m} \sum_{k=1}^m b_k - b_0 \\ &\approx \frac{1}{n} \sum_{R_i \subset V_0} b(\mathbf{R}_i) - b_0. \end{aligned} \tag{2.12}$$

Its variance is

$$\begin{aligned} \nu_\nu &= \text{var}(\Delta b_\nu) \\ &= \frac{1}{m} \sum_{k=1}^m \text{var}(b_k) \\ &= \frac{1}{m} \sum_{k=1}^m \nu_k. \end{aligned} \tag{2.13}$$

So, correspondingly, the estimate of ν_ν can be given as

$$\tilde{\nu}_\nu = \frac{1}{m} \sum_{k=1}^m \tilde{\nu}_k = M_w. \tag{2.14}$$

The test statistic is⁷

$$\hat{t} = \frac{\Delta b_\nu}{\sqrt{\tilde{\nu}_\nu}} = \frac{\Delta b_\nu}{\sqrt{M_w}}, \tag{2.15}$$

which has $\nu = mN_e$ degrees of freedom. If $\hat{t} > t_{\nu,\alpha}$, $\bar{b}_\nu > b_0$ can be accepted at the α level. $t_{\nu,\alpha}$ is the t -test threshold that is tabulated in standard statistics books. Note that the one-sided test is used here.

For $N \geq 60$ (and consequently $\nu \geq 30$; see Subsection 2.A.2) and $\alpha \in (0.01, 0.5)$, the threshold $t_{\nu,\alpha}$ deviates from the normal distribution n_α by only $\leq 5\%$. So n_α can be used for $t_{\nu,\alpha}$ in the above statistical tests, which avoids having to estimate N_e . The two commonly used confidence levels in this one-sided test are $n_{0.05} = 1.65$ and $n_{0.01} = 2.35$.

B. Significance of Structural Differences between Related Objects

There are cases in which reconstructions are done for different preparation methods or from particles with small (or local) conformational differences, e.g., because of ligand binding or channel closing–opening. The question then arises, how significant is the difference of certain

features in the two reconstructions? This question can be answered by rigorous statistical tests based on the knowledge of the 3-D variance estimates.

1. Voxelwise Comparison

Let $b_1(\mathbf{R})$ and $b_2(\mathbf{R})$ be two independent reconstructions derived from two projection sets that contain N_1 and N_2 images, respectively. If we assume that their variance estimates $\bar{\nu}_1(\mathbf{R})$ and $\bar{\nu}_2(\mathbf{R})$ have χ^2 distributions with NDF N_{e1} and N_{e2} , respectively, that is,

$$\text{var}[\bar{\nu}_i(\mathbf{R})] = \frac{1}{N_{ei}} \nu_i^2(\mathbf{R}), \quad (2.16)$$

then the condition of equal sample variances⁷ is equivalent to

$$(N_{e1} + 1)\nu_1^2(\mathbf{R}) = (N_{e2} + 1)\nu_2^2(\mathbf{R}). \quad (2.17)$$

However, because this condition is generally not valid, the test statistic for possibly unequal variances should be used:

$$\hat{t}(\mathbf{R}) = \frac{|b_1(\mathbf{R}) - b_2(\mathbf{R})|}{[\bar{\nu}_1(\mathbf{R}) + \bar{\nu}_2(\mathbf{R})]^{1/2}}, \quad (2.18)$$

where the NDF is the rounded-off value of

$$\nu(\mathbf{R}) = \frac{[\bar{\nu}_1(\mathbf{R}) + \nu_2(\mathbf{R})]^2}{\frac{\bar{\nu}_1^2(\mathbf{R})}{N_{e1}} + \frac{\bar{\nu}_2^2(\mathbf{R})}{N_{e2}}}. \quad (2.19)$$

If $\hat{t}(\mathbf{R}) > t_{\nu, \alpha}$, $b_1(\mathbf{R}) \neq b_2(\mathbf{R})$ can be accepted at the α level.

As in the discussion in Subsection 2.A.3, n_α can be used for $t_{\nu, \alpha}$ in the above statistical test to avoid having to estimate N_{e1} and N_{e2} . The two commonly used confidence levels in this two-sided test are $n_{0.05} = 1.96$ and $n_{0.01} = 2.58$.

2. Comparison of Corresponding Local Features

Note that in the above analysis in Subsection 2.B.1, corresponding voxels in the two 3-D images are compared pairwise, irrespective of the behavior of the other voxels in the reconstructions. We now discuss the effects of feature size and low-pass cutoff frequency on the t -test map to answer the question about the significance of differences between local features in two reconstructions.

The question of comparing two uniform local features situated at \mathbf{R}_0 within the probing volume V_0 in two 3-D images can be phrased as the significance assessment of the difference between the averages $\bar{b}_1 \equiv 1/V_0 \int_{\mathbf{R} \in V_0} b_1(\mathbf{R}) d^3\mathbf{R}$ and $\bar{b}_2 \equiv 1/V_0 \int_{\mathbf{R} \in V_0} b_2(\mathbf{R}) d^3\mathbf{R}$ with the test statistic

$$\hat{t} = \frac{|\bar{b}_1 - \bar{b}_2|}{(\bar{\nu}_1 + \bar{\nu}_2)^{1/2}}, \quad (2.20)$$

where $\bar{\nu}_L$ ($L = 1, 2$) is the variance estimate of \bar{b}_L . Now the question becomes how to obtain $\bar{\nu}_L$, which generally requires the knowledge of the covariance between the voxels within V_0 . Below we discuss two practical ways of getting around the use of the covariance:

(i) The resolution filtration function corresponds to a low-pass filter (with the cutoff frequency U_f) that implicitly performs local averaging. Hence, when a feature at

\mathbf{R}_0 in the object has a size of $< 1/(2U_f)$, then, owing to the missing cone¹ effect, the corresponding feature in the reconstruction will have a roughly ellipsoidal shape with the widths of $1/(2U_f)$ in the $X - Y$ direction and of $\epsilon/(2U_f)$ in the Z direction. Hence $\bar{b}_L \approx b_L(\mathbf{R}_0)$ and, correspondingly, $\bar{\nu}_L \approx \nu_L(\mathbf{R}_0)$. This actually means that, for the comparison of features of size $1/(2U_f)$ at \mathbf{R}_0 , we can conveniently check the value at this point in the t -test map with the cutoff frequency U_f . Therefore, to check the significance of differences between local features of different size ranges, we propose computing a number of 3-D variance estimates and corresponding t -tests with different cutoff frequencies.

(ii) Another way, which is valid for assessing a uniform feature with any shape and requires a short correlation range of projection noise, is to count the effect of the above covariance by the use of the NDF of this feature, as discussed in Subsection 2.A.1, such that

$$\nu_L \approx \frac{1}{m} \bar{\nu}_L \equiv \frac{1}{m} \left[\frac{1}{V_0} \int_{\mathbf{R} \in V_0} b_1(\mathbf{R}) d^3\mathbf{R} \right]. \quad (2.21)$$

Its estimate ν_L is obtained through the substitution of $\nu_L(\mathbf{R})$ by $\bar{\nu}_L(\mathbf{R})$.

3. APPLICATION OF VARIANCE ANALYSIS TO HEMOCYANIN-FAB COMPLEX EPITOPE LOCALIZATION IN THREE DIMENSIONS

3-D immunoelectron microscopy⁸ offers a way to localize a short segment of a polypeptide chain on the surface of the folded protein (the antigen): both the native protein molecule⁹ and the same molecule complexed with a site-specific, monoclonal antibody are imaged with the electron microscope, reconstructed in three dimensions, and a difference map is computed. In this map, only a small portion of the Fab immediately in contact with the binding site (the epitope) is revealed as a peak, whereas the bulk of the mass is invisible since it is blurred because of the rotational movement of the Fab arm around the binding site.

This method of epitope localization is the only one available for large macromolecular complexes that are difficult to grow into crystals that are amenable to x-ray crystallographic analysis. In cases in which the structure of a subunit is known by x-ray analysis, the combination of data from 3-D immunoelectron microscopy and x-ray crystallography has the potential of providing near-atomic resolution.

The hemocyanin of the horseshoe crab *Androctonus australis* is a large oligomeric complex made up of 24 subunits that occur in groups of six and that are drawn from eight different subunit types (Fig. 2). Subunit Aa6, the antigen for the present immunoelectron microscopy study, occurs in four symmetrically located copies. The data set used in the present study was part of a larger data set obtained by Boisset *et al.* in their effort to localize the L104 antibody to an epitope on the surface of Aa6.⁸

In that study, which followed the protocol of the random-conical reconstruction,¹⁰ the specimen was first imaged with a tilt angle of 50°, then without tilt. The resulting 21 pairs of micrographs were digitized, and particle images were extracted pairwise and aligned.

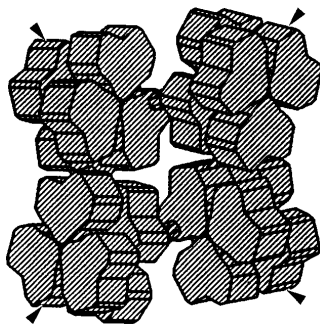


Fig. 2. Model of the quaternary structure of scorpion *Androctonus australis* hemocyanin from its top view in which the molecule lies on its flip face. *A. australis* hemocyanin is a copper-containing oxygen carrier that has a 4×6 -mer structure. Its 24 subunits belong to eight different polypeptide chains with a molecular weight of 75 kDa each. The molecule possesses a twofold axis of symmetry passing through its center. Because of the noncoplanar arrangement of the hexameric building blocks, the molecule is able to rock around an axis that passes through the two diagonally opposed axes on the grid.⁹ The locations of the IgG 104 antibody epitopes on the four copies of subunit Aa6 are shown by arrows (reprinted from Ref. 9, with permission from Academic Press).

Classification was applied to the 0° projections in order to isolate 404 molecules that presented the same orientation, the flip-top view. Molecules that presented the opposite view, the flop-top view, were disregarded in the current study.

Altogether, four binding sites are available on the whole hemocyanin molecule (Fig. 2). In practice, not all of these are always occupied, and therefore immunocomplexes with sites 0, 1, 2, 3, and 4 bound with Fab are encountered. We isolated two classes with the following properties:

Class I: no Fab at site 1, but Fab's with varying frequencies at sites 2, 3, and 4 (total of 109).

Class II: Fab at all four sites (total of 184).

These classes are mutually exclusive, a property that guarantees that their variances are independent. This property is important in the application of the *t*-test below. (The remaining molecules, not considered as a separate class in the following, have site 1 always occupied but at least one other site unoccupied.)

From the tilted-specimen projections, three reconstructions were done: one (labeled *T* for total below) from the total set of flip-top views, and one each from the images falling into classes I (termed I) and II (termed II), respectively.

Below we focus our attention on site 1. The percentages of absences of Fab's from sites 1, 2, 3, and 4 are 28%, 12%, 17%, and 11%, respectively. In reconstruction I, site 1 is consistently unoccupied, whereas it is consistently occupied in reconstruction II. Localization can now go by two routes: (A) computing the 3-D difference map $(II) - (I)$ and investigating the significance of the difference peak by the use of 3-D variance maps for I and II, or (B) computing the 3-D variance map that corresponds to reconstruction *T*.

A. Difference Map and Evaluation of Significance

From the way the particles were classified, the ratio of occupancies between classes I and II is 0:100 for site 1,

while it is in the range of 80:100 to 100:100 for sites 2–4. Consequently, all Fab's that show up in the two reconstructions [sites 1–4 for class II, Fig. 3(a), and sites 2–4 for class I, Fig. 3(b)] appear with virtually the same intensity. For the same reason, the difference map $(II) - (I)$ shows only the Fab fragment bound to site 1 but no trace of Fab's at the other sites.

The precise binding site can be established by the superposition of the difference map onto (II), but a quantitative determination of the boundary between the Fab and the antigen requires a voxel-by-voxel *t*-test in three dimensions. This has been achieved in Fig. 3(f) by the use of Eq. (2.15) with the two 3-D variance estimates [Figs. 3(d) and 3(e)] that were obtained after preconstruction low-pass filtration cutoff of $1/(31.1 \text{ \AA})$ to the two sets of projections was employed.

In the *t*-test map, which describes the regions of the most significant differences, the boundary of the Fab fragment is sharply delineated. Other small spots of high significance in the region of the antigen can be explained as instances of the type-II error⁶ (e.g., there is no structural difference but a significance of difference is claimed). However, most of these spots correspond to the lower confidence level of 95%. Superposition of the *t*-test map onto the reconstruction (not shown) provides the most accurate determination of the epitope site available with 3-D electron microscopy.

X-ray crystallography has shown that the Fab antibody fragment has a central hinge region,¹¹ and stain

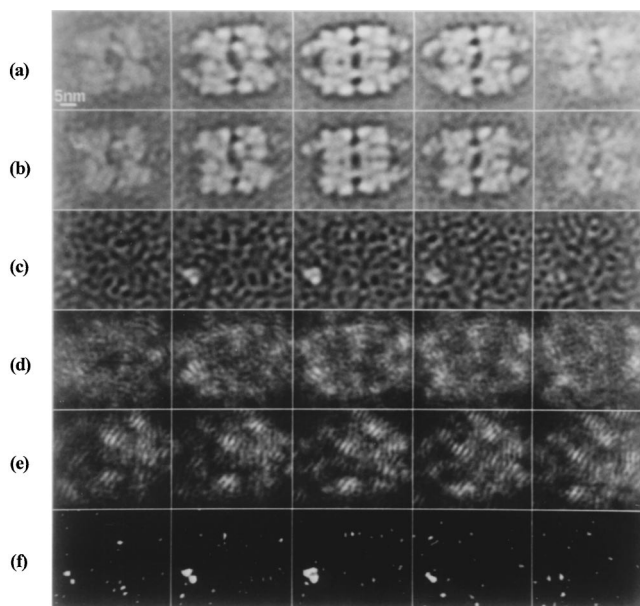


Fig. 3. Significance assessment of difference between reconstructions of class-II and class-I hemocyanin-Fab complex by the use of the *t*-test: (a), (b) *Z*-slice montages of 3-D reconstructions of class II and class I, respectively, with the cutoff frequency of low-pass filter $U_f = 1/(31.1 \text{ \AA})$ and the number of projections $N_2 = 184$ and $N_1 = 109$; (c) *Z*-slice montage of the 3-D difference map from the reconstructions of class II and class I as shown in (a) and (b), respectively; (d), (e) *Z*-slice montages of 3-D variance estimates of class II and class I, respectively; (f) montage of the 3-D *t*-test map of the differences as shown in (c), with bright areas corresponding to the significance level of 99%, where $\hat{t}(R_\perp) > n_{0.01}$, and bright plus gray areas corresponding to 95%, where $\hat{t}(R_\perp) > n_{0.05}$. The distance between consecutive slices is 15.6 \AA for all the montages in Figs. 3 and 4.

is expected to accumulate at this point in the electron microscopic preparation. It is remarkable that, despite the mobility of the Fab fragment around the binding site (see below for evidence in the variance map of reconstruction T), the stain deposited in this hinge region is visualized both in the 3-D difference map and in the t -test map.

B. Variance Map of the Total Particle Set and Assessment of Conformational Changes

From its definition, the meaning of the 3-D variance estimate is the (voxelwise) variance of the 3-D image, not of the particle itself. Nevertheless, because a substantial part of the noise contributed to the 3-D image by the projections is due to the particle's conformational variations, these variations are reflected in the estimated variance map. In our companion paper¹ we have analyzed these contributions with the aid of a simple model. In attempting to attribute highlights in the variance map to local conformational changes, we also must keep in mind the statistical uncertainty of the 3-D variance estimate itself. By making use of certain conjectures based on the theory of variance estimation, we can formulate a rule of thumb (see Appendix A): essentially, such a highlight may reflect a conformational change, unless (i) it originates from a single backprojection ray (i.e., from a single projection) and (ii) its value is not significantly above the level of background granularity. In general, the uncertainty in this interpretation can be reduced if the total number of projections is increased.

Figure 4 shows equivalent slices of two reconstructions and corresponding variance estimates. The use of low-pass filters with different radii U_f before reconstruction results in a focus on different aspects of conformational variation characterized by the size $d = 1/U_f$. This selective property of low-pass filtration is the combined result of the fact that the spectral noise energy increases with increasing spatial frequency and that the total contribution of noise energy from any spatial frequency band is proportional to the radius of that band. In the case of the hemocyanin-Fab complex, the 3-D average variance obtained with $U_f = 1/31 \text{ \AA}^{-1}$ [Fig. 4(d); reconstruction in Fig. 4(c)] is four times that with $U_f = 1/47 \text{ \AA}^{-1}$ [Fig. 4(b); reconstruction in Fig. 4(a)]. ($0.1 \text{ \AA} = 1 \text{ nm}$.)

There are six variance highlights visible in Figs. 4(b) and 4(d) that stand out from the background and that are not caused by single projection lines. These are located at the sites of the four Fab arms and at two staining pits that lie on the vertical line that divides the molecule. Essentially the variance highlights reflect three different variational effects: (i) presence or absence of a structural component. We know that the largest effect of this kind occurs at the lower left-hand corner, as here the two major classes, I and II, differ in the presence versus absence of an Fab. However, we note that the variance highlight at that corner does not stand out from those at the other corners; (ii) positional variations of a structural component. The Fab's essentially swing around their four binding sites. This effect is responsible for the fact that each variance highlight accompanying an Fab is smeared out over an area larger than the area occupied by the averaged Fab; (iii) finally, variation in stain depth. Here an entire stain-filled region varies in inten-

sity, and the result is a variance highlight that is more or less shaped like that region [see in particular Fig. 4(c)].

For class II with 100% occupancies on all four Fab binding sites, the above variational case (i) is excluded. Hence a Fab's positional variations should be indicated by two adjacent highlights at the binding site. This is indeed the case as shown in Fig. 4(f).

Therefore both the total class and class II indicate the existence of conformational changes at the Fab binding sites by variance highlights. But if the question is whether the changes follow cases (i), (ii), or both, only a double peak will unambiguously point to case (ii). This is exactly the situation that was analyzed in the preceding paper¹ by the use of a model of two 3-D point noise sources.

4. DISCUSSION

Application to the hemocyanin-Fab complex demonstrates the power of the variance estimation method as a way of pinpointing sites of conformational variability or experimental changes. Variance estimation also addresses a fundamental problem of 3-D electron microscopy of single macromolecules, a technique that relies on the validity of the classification of molecules based solely on their projections.¹² The inherent ambiguity of this approach can be resolved when variance maps are computed for each reconstruction.

Classification and variance analysis represent complementary tools for dealing with heterogeneity in a data set.¹³ Their roles are in some respects complementary, in some respects antagonistic: as the scrutiny of classification increases, resulting in an increased number of

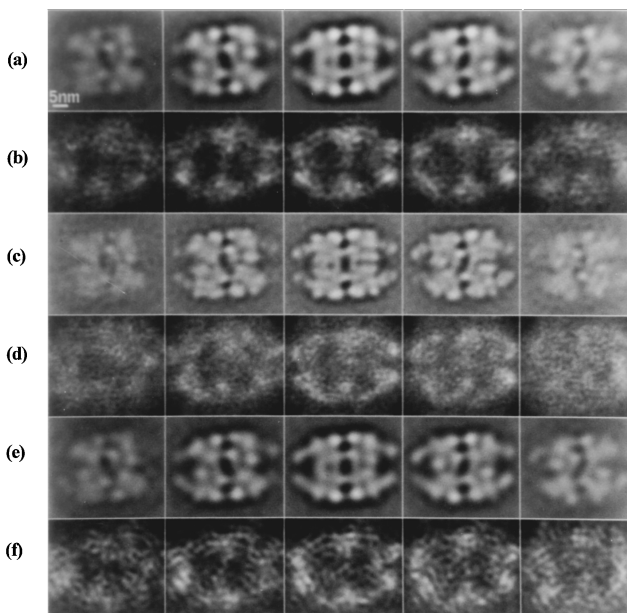


Fig. 4. Z-slice montages of 3-D reconstructions and corresponding 3-D variance estimates of the hemocyanin-Fab complex: (a)–(d) correspond to the total flip-top data set for two frequency cutoffs U_f of the low-pass filter. The majority of the $N_T = 404$ projections have Fab bound to each of the four sites. (a), (b) Reconstruction and 3-D variance estimate for $U_f = 1/(46.7 \text{ \AA})$; (c), (d) reconstruction and 3-D variance estimate for $U_f = 1/(31.1 \text{ \AA})$; (e), (f) reconstruction and 3-D variance estimate of class II for $U_f = 1/(46.7 \text{ \AA})$.

classes, the variance of each class reconstruction will be reduced. Conversely, a larger latitude in the classification resulting in only a few classes produces 3-D images with internal inconsistencies that show up prominently in the variance map.

5. CONCLUSIONS

A 3-D variance estimation theory has been developed and has been successfully applied to the study of a macromolecular assembly. The location of regions with high structural variability were found to be reflected by high values in the 3-D variance map. The structural differences between reconstructions of different classes could be assessed by the use of the statistical *t*-test or by the examination of the 3-D variance map of the mixed class. The combination of classification analysis, 3-D reconstruction, and 3-D variance estimation has been shown to be powerful in immunoelectron microscopy, for which it provides information about the structure and the conformational variability of the immunocomplex and yields the locations of the 3-D antibody binding sites. Our analysis has thus laid the foundation for practical applications of the 3-D variance to the structural studies of biological macromolecules.

APPENDIX A: RULE FOR VISUALLY IDENTIFYING A THREE-DIMENSIONAL CONFORMATIONAL CHANGE BY THE INSPECTION OF THE THREE-DIMENSIONAL VARIANCE MAP

The projections in a set can be collected from particles with different conformational states. Thus the detectability of a conformational change from the 3-D variance map depends on

- (i) its size and magnitude relative to the background noise,
- (ii) its frequency of occurrence,
- (iii) whether or not it is a well-isolated region (that is, whether the surrounding conformational motifs will or will not interfere),
- (iv) whether the number of projections is large enough to suppress the statistical uncertainty of the 3-D variance estimate and the interference by outliers.

The relationship between, and the effects of, these factors can be illustrated by the analysis of a population of dual conformational states: suppose, for a given projection set, that the corresponding particles have two conformational states, P_o and P_c . This can be channel opened or closed, for example. If P_c is so rare that only one or two P_c projections appear in a set of N projections, and if the difference between P_o and P_c is significantly above the background noise level, then P_c projections will contribute backprojection lines across the 3-D variance. But in practice, one cannot tell if P_c is a true but rare conformational state or an artifact. If it can only interfere with obtaining additional information on the P_o state, the rare projection should be regarded as an outlier and be rejected.

If a sizable number of such P_c projections (10, say) appear in a set of $N > 100$, the corresponding backprojection lines will converge to one point in the 3-D variance.

This point of convergence will be a bright spot above the background, which tells us that these lines are not likely due to artifacts but rather are a reflection of a possible conformational change.

If P_c projections form 50% of the total set of a given set of N , then the conformational change will be fully expressed in the 3-D variance. Statistically, the flexible region of the particle in the 3-D variance map will then be its brightest possible.

For a fixed number of projections, a projection set that contains both P_o and P_c states will introduce an extra 3-D variance component $\Delta\nu(\mathbf{R})$, adding to the 3-D variance $\nu_o(\mathbf{R})$ of a pure P_o set. Model analysis shows that

$$\Delta\nu(\mathbf{R})/\nu(\mathbf{R}) = \frac{\Delta\nu(\mathbf{R})}{\nu_o(\mathbf{R}) + \Delta\nu(\mathbf{R})} \propto P_c(1 - P_c). \quad (\text{A1})$$

So already 12.5% P_c -state projections in a set contribute to $\Delta\nu(\mathbf{R})$ almost half as much as 50% projections do. This implies that if a projection data set comprises two conformational states, its existence will already be manifested in the 3-D variance map as long as the minority state population is not quite rare, whereas a 50/50 situation gives the optimum detectability.

Below we discuss the effect of the number of projections N on the significance of a high-density variance region that represents conformational changes. When the projection distribution satisfies the sampling rate requirement within the range of radius U_f in 3-D Fourier space,

$$\nu(\mathbf{R}) \propto \frac{1}{N}. \quad (\text{A2})$$

The statistics of 3-D variance estimate $\hat{\nu}(\mathbf{R})$ is¹

$$\text{var}[\hat{\nu}(\mathbf{R})]/\nu(\mathbf{R}) = \sqrt{\frac{2}{N_e}} \propto \frac{1}{\sqrt{N}}, \quad (\text{A3})$$

where N_e is the NDF of $\hat{\nu}(\mathbf{R})$.

For a true outlier, only one such motif is present in the set, and its corresponding extra variance component $\nu_{\text{out}}(\mathbf{R})$ has

$$\nu_{\text{out}}(\mathbf{R})/\nu(\mathbf{R}) \propto \frac{1}{N}. \quad (\text{A4})$$

In contrast, a local maximum that reflects the conformational changes produces

$$\Delta\nu(\mathbf{R})/\nu(\mathbf{R}) = \text{const}, \quad (\text{A5})$$

which is due to its recurring nature.

So although the 3-D variance decreases with $1/N$ while the relative statistical uncertainty of 3-D variance estimation decreases with $1/\sqrt{N}$ and the contribution of an outlier is suppressed at the pace of $1/N$, the relative prominence of a conformational change stays nevertheless constant.

Therefore, with an increasing number of projections, outliers will be suppressed while a true conformational change stands out from background fluctuations of the 3-D variance. This implies the rule for visually identifying a conformational change by the inspection of the 3-D variance distribution: if a high-density spot or re-

gion stands out from background variance fluctuations and is not derived from a single backprojection ray, it is likely to be the reflection of conformational change in that region.

ACKNOWLEDGMENTS

We gratefully acknowledge discussions with Pawel Penczek. This work was supported by National Institutes of Health grants NIH 1 R01 GM 29169 and NIH 1 S10 RR0399801 to principal investigator J. Frank.

*Present address, ATS/WATCHER Division, KLA Instruments Corporation, 160 Rio Robles, P.O. Box 49055, San Jose, California 95161-9055.

REFERENCES

1. W. Liu and J. Frank, "Estimation of variance distribution in three-dimensional reconstruction. I. Theory," *J. Opt. Soc. Am. A* **12**, 2615-2627 (1995).
2. J. Frank, A. Verschoor, and M. Boublik, "Computer averaging of 40S ribosomal subunits," *Science* **214**, 1353-1355 (1981).
3. W. O. Saxton and W. Baumeister, "The correlation averaging of a regularly arranged bacterial envelope protein," *J. Microsc.* **127**, 127-128 (1982).
4. M. Unser, B. L. Trus, and A. C. Steven, "A new resolution criterion based on spectral signal-to-noise ratios," *Ultra-microscopy* **23**, 39-42 (1987).
5. W. Hänicke, J. Frank, and H. P. Zingsheim, "Statistical significance of molecule projections by single particle averaging," *J. Microsc.* **133**, 223-238 (1984).
6. L. Sachs, *Applied Statistics, A Handbook of Techniques*, 2nd ed. (Springer-Verlag, New York, 1984).
7. E. J. Dudewicz and S. N. Mishra, *Modern Mathematical Statistics*, Vol. 19 of Wiley Series in Probability and Mathematical Statistics (Wiley, New York, 1988).
8. N. Boisset, M. Radermacher, R. Grassucci, J. C. Taveau, W. Liu, J. Lamy, J. Frank, and J. N. Lamy, "Three-dimensional immunoelectron microscopy of scorpion hemocyanin labeled with a monoclonal Fab fragment," *J. Struct. Biol.* **111**, 234-244 (1993).
9. N. Boisset, J. C. Taveau, J. Lamy, T. Wagenknecht, M. Radermacher, and J. Frank, "Three-dimensional reconstruction of native *Androctonus australis* hemocyanin," *J. Mol. Biol.* **216**, 743-760 (1990).
10. M. Radermacher, "Three-dimensional reconstruction of single particles from random and nonrandom tilt series," *J. Electron Microsc. Tech.* **9**, 359-394 (1988).
11. R. J. Poljak, L. M. Amzel, H. P. Avey, L. N. Becha, and A. Nisonoff, "Structure of Fab' new at 6 Ångstroems resolution," *Nature/New Biology (London)* **235**, 137-141 (1972).
12. J. Frank, "Classification of macromolecular assemblies studied as 'single particles'," *Q. Rev. Biophys.* **23**, 281-329 (1990).
13. J. Frank, W. Liu, and N. Boisset, "Classification and 3D variance estimation: complementary tools in the 3D reconstruction of macromolecules," in *Proceedings of the 10th European Congress on Electron Microscopy* (Secretariado de Publicaciones de la Universidad de Granada, Granada, Spain, 1992), pp. 427-429.